

Anisotropic metal–insulator transition in strained VO_2(B) single crystal

Zecheng Ma(马泽成), Shengnan Yan(闫胜楠), Zenglin Liu(刘增霖), Tao Xu(徐涛), Fanqiang Chen(陈繁强), Sicheng Chen(陈思成), Tianjun Cao(曹天俊), Litao Sun(孙立涛), Bin Cheng(程斌), Shi-Jun Liang(梁世军), and Feng Miao(缪峰)

Citation: Chin. Phys. B, 2024, 33 (**6**): 067103. DOI: 10.1088/1674-1056/ad39d4
Journal homepage: http://cpb.iphy.ac.cn; http://iopscience.iop.org/cpb

What follows is a list of articles you may be interested in

Design of sign-reversible Berry phase effect in 2D magneto-valley material

Yue-Tong Han(韩曰通), Yu-Xian Yang(杨宇贤), Ping Li(李萍), and Chang-Wen Zhang(张昌文)
Chin. Phys. B, 2023, 32 (**9**): 097101. DOI: 10.1088/1674-1056/acd920

Symmetry-constrained quantum coupling in non-Fermi-liquid transport

Rong Li(李荣) and Zhen-Su She(佘振苏)
Chin. Phys. B, 2023, 32 (**6**): 067104. DOI: 10.1088/1674-1056/acc0f4

Coexistence of giant Rashba spin splitting and quantum spin Hall effect in H-Pb-F

Wenming Xue(薛文明), Jin Li(李金), Chaoyu He(何朝宇), Tao Ouyang(欧阳滔), Xiongying Dai(戴雄英), and Jianxin Zhong(钟建新)
Chin. Phys. B, 2023, 32 (**3**): 037101. DOI: 10.1088/1674-1056/aca7eb

Blue phosphorene/$MoSi_2N_4$ van der Waals type-II heterostructure: Highly efficient bifunctional materials for photocatalytics and photovoltaics

Xiaohua Li(李晓华), Baoji Wang(王宝基), and Sanhuang Ke(柯三黄)
Chin. Phys. B, 2023, 32 (**2**): 027104. DOI: 10.1088/1674-1056/ac9469

In situ electronic structural study of VO_2 thin film across the metal–insulator transition

Emin Muhemmed (伊明江·买买提), Abduleziz Ablat (阿布都艾则孜·阿布来提), Wu Rui (吴蕊), Wang Jia-Ou (王嘉鸥), Qian Hai-Jie (钱海杰), Kurash Ibrahim (奎热西·依布拉欣)
Chin. Phys. B, 2013, 22 (**12**): 127103. DOI: 10.1088/1674-1056/22/12/127103

RAPID COMMUNICATION

Anisotropic metal–insulator transition in strained VO_2(B) single crystal

Zecheng Ma(马泽成)[1,†], Shengnan Yan(闫胜楠)[1,†], Zenglin Liu(刘增霖)[1], Tao Xu(徐涛)[2], Fanqiang Chen(陈繁强)[1], Sicheng Chen(陈思成)[1], Tianjun Cao(曹天俊)[1], Litao Sun(孙立涛)[2], Bin Cheng(程斌)[3], Shi-Jun Liang(梁世军)[1,‡], and Feng Miao(缪峰)[1,§]

[1] *Institute of Brain-Inspired Intelligence, National Laboratory of Solid State Microstructures, School of Physics, Collaborative Innovation Center of Advanced Microstructures, Nanjing University, Nanjing* 210093, *China*

[2] *SEU-FEI Nano-Pico Center, Key Laboratory of MEMS of Ministry of Education, Southeast University, Nanjing* 210096, *China*

[3] *Institute of Interdisciplinary of Physical Sciences, School of Science, Nanjing University of Science and Technology, Nanjing* 210094, *China*

(Received 15 February 2024; revised manuscript received 20 March 2024; accepted manuscript online 3 April 2024)

Mechanical strain can induce noteworthy structural and electronic changes in vanadium dioxide, imparting substantial scientific importance to both the exploration of phase transitions and the development of potential technological applications. Unlike the traditional rutile (R) phase, bronze-phase vanadium dioxide [VO_2(B)] exhibits an in-plane anisotropic structure. When subjected to stretching along distinct crystallographic axes, VO_2(B) may further manifest the axial dependence in lattice–electron interactions, which is beneficial for gaining insights into the anisotropy of electronic transport. Here, we report an anisotropic room-temperature metal–insulator transition in single-crystal VO_2(B) by applying *in-situ* uniaxial tensile strain. This material exhibits significantly different electromechanical responses along two anisotropic axes. We reveal that such an anisotropic electromechanical response mainly arises from the preferential arrangement of a strain-induced unidirectional stripe state in the conductive channel. This insulating stripe state could be attributed to the in-plane dimerization within the distorted zigzag chains of vanadium atoms, evidenced by strain-modulated Raman spectra. Our work may open up a promising avenue for exploiting the anisotropy of metal–insulator transition in vanadium dioxide for potential technological applications.

Keywords: vanadium dioxide, strain, anisotropy, electrical transport

PACS: 71.30.+h, 72.80.Ga, 78.20.−e, 07.10.Pz **DOI:** 10.1088/1674-1056/ad39d4

Strain plays a crucial role in controlling the electrical, optical and magnetic properties of strongly correlated materials by means of coupling various degrees of freedom (i.e., lattice, electron and orbital).[1–3] As a conventional strongly correlated material, vanadium dioxide (VO_2) has attracted tremendous attention for the strain engineering in consequence of the rich variety of structures, along with its well-known metal–insulator transition (MIT).[4–6] In the most studied rutile VO_2(R), research has demonstrated that epitaxial strain can influence the MIT behaviors,[7,8] and induce the phase separation,[9–11] which makes a significant contribution to understanding the phase transition mechanism. Application of a sufficiently large tensile strain can induce another monoclinic (M2) insulating phase, accompanied by the different dimerization of vanadium chains from that reported in the room-temperature monoclinic (M1) insulating phase.[12] Moreover, the investigation of critical phenomena in phase transitions can be facilitated by the *in-situ* accurate control of strain.[13–16]

Differing from the most studied VO_2(R), bronze-phase vanadium dioxide [VO_2(B)] possesses a distinct lattice structure and physical properties. Such diversities can be attributed to the different distortions and arrangements of VO_6 octahedra, as well as the various coordination and dimerization of vanadium atoms. It has been demonstrated that VO_2(B) exhibits a monoclinic metallic state at room temperature and undergoes a MIT below 240 K, characterized by a first-order thermal hysteresis and the formation of vanadium dimers.[17–22] Besides, VO_2(B) exhibits a large degree of structural anisotropy,[23] facilitating the study of anisotropic electronic transport. As a sensitive means, uniaxial mechanical strain may effectively induce lattice deformation along two anisotropic directions of VO_2(B) and cause profound changes in its electronic structure, which presents an unparalleled opportunity for a deeper understanding of anisotropy physics.

In this work, we report the discovery of a strain-induced anisotropic MIT in synthesized single-crystal VO_2(B) flakes. We apply uniaxial tension along in-plane anisotropic axes respectively to present an in-depth comparison of electromechanical properties. Two crystallographic directions of VO_2(B) exhibit distinctly disparate resistance responses to the applied mechanical strain. We uncover that the observed difference may result from a novel dimerization mechanism due

[†]These authors contributed equally to this work.

[‡]Corresponding author. E-mail: sjliang@nju.edu.cn

[§]Corresponding author. E-mail: miao@nju.edu.cn

© 2024 Chinese Physical Society and IOP Publishing Ltd

to the deformation of zigzag chains in the VO_2(B) lattice, as evidenced by the strain-modulated Raman spectra. Our study provides a new strategy to explore the phase transition mechanism in vanadium dioxide.

Monoclinic VO_2(B) is a thermodynamically metastable phase, which belongs to the $C2/m$ space group.[24,25] The unit cell of VO_2(B) exhibits a typical layered-like structure, as shown in the dashed box of Fig. 1(a). Each layer consists of two sublayers of distorted VO_6 octahedra and stacks with neighboring layers through corner sharing along the [001] direction, giving rise to a three-dimensional framework. In the (001) plane (*ab* plane), two different types of off-centered VO_6 octahedra at V(1) and V(2) atom sites, respectively, share edges and connect alternately, forming zigzag chains along the [010] direction (*b*-axis). The duplex zigzag chain of vanadium atoms links to adjacent chains along the [100] direction (*a*-axis) via edge-sharing V(2) octahedra of two sublayers, leading to the pronounced structural anisotropy within the *ab* plane. Furthermore, the inherent susceptibility of the zigzag chains to uniaxial strain renders the VO_2(B) single crystal an ideal candidate for in-depth research into its anisotropic electromechanical coupling.

The high-quality and pure-phase VO_2(B) flakes were grown on SiO_2/Si substrate. A typical single-crystal VO_2(B) sample is demonstrated in Fig. 1(b), which commonly possesses two parallel long edges. The atomic force microscopy (AFM) reveals the sample thickness of 36.5 nm and the surface roughness within 0.5 nm, indicating outstanding flatness and uniformity. To confirm the crystallinity and the crystal orientation, we utilized high-resolution transmission electron microscopy (HRTEM) to characterize multiple as-grown VO_2(B) flakes. The HRTEM image illustrates the ordered arrangement of vanadium atoms and unequivocally indicates its nature of single crystal [Fig. S1 and Fig. 1(c)]. The corresponding diffraction pattern obtained through fast Fourier transform (FFT) analysis reveals that the long edge direction is uniformly perpendicular to the (200) plane, affirming its alignment with the *b*-axis.

In order to facilitate the *in-situ* study of electromechanical properties, we directly transferred the synthesized VO_2(B) flakes (30 nm–60 nm) onto a flexible and insulating polyimide membrane, known for its remarkable mechanical resilience and thermal stability. Subsequently, we carried out the standard procedures of electron-beam lithography and deposition to fabricate two- or four-terminal electrodes, composed of 5 nm titanium (Ti) and 80 nm gold (Au). The preparative VO_2(B) device was bonded to a custom-made socket and loaded onto a strain setup, which is based on a pushing-needle system controlled by a precision positioner (Fig. S2). According to the three-point bending geometry, a uniaxial tensile strain could be generated on the upper surface of the polyimide substrate under the vertical squeeze of the pushing needle. Further, due to the clamping function of the metal electrodes, strains can be effectively transferred to the VO_2(B) devices along various crystallographic directions, as shown in Fig. 1(d). Consistent with our previous study,[26] the continuously adjustable strain (ε) via substrate bending can be quantitatively described as $\varepsilon = n/(h + w^2/h - n)$, where n is the polyimide substrate thickness, h is the vertical displacement of the pushing needle, and w is the half distance between two PCB supports of the socket.

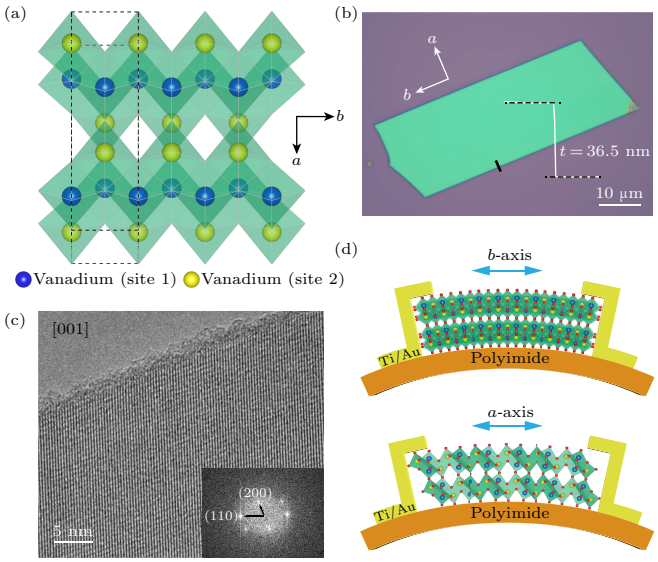


Fig. 1. (a) Lattice structure of a VO_2(B) single layer along the [001] direction. The deliberate omission of oxygen atoms situated at the terminals of VO_6 octahedra is aimed at facilitating clearer observation. (b) Optical image of a single-crystal VO_2(B) flake with the thickness of 36.5 nm on a SiO_2/Si substrate. (c) HRTEM image near the long edge of a VO_2(B) flake. The inset shows the corresponding FFT pattern. (d) Schematic of VO_2(B) flexible devices under the uniaxial tensile strain along the *b*-axis (top) and the *a*-axis (bottom), respectively.

We characterized the electromechanical responses of two VO_2(B) devices subjected to various uniaxial tensile strains. Without any constraint, the device along the zigzag direction (i.e., *b*-axis) exhibits a low electrical resistivity of 3.6×10^{-3} Ω·cm. As the upward-moving pushing needle bends the flexible substrate, corresponding to an increase in tensile strain, the normalized resistance only attains a small value of 3 at 0.33% strain [Fig. 2(a)]. When a strain of 0.38% is applied, the normalized resistance ramps up and commences a linear increase. Ultimately, the resistance amplifies over a thousand-fold from the original value at 1.31% strain, resulting in a transition from an initial metallic state to an insulating state. In contrast, when the increasing strain is oriented perpendicular to the zigzag chains of vanadium atoms (i.e., along the *a*-axis), the VO_2(B) device shows a significantly different electromechanical response [Fig. 2(b)]. This device exhibits an unstrained resistivity of 7.0×10^{-3} Ω·cm and a small increment over a broader strain range. Upon reaching 0.95% strain, the normalized resistance starts to increase rapidly, and

a dramatic surge from 139 to 1188 occurs within a narrow strain range of 0.08% (from 0.99% to 1.07%). After the sharp jump, the resistance, which has a large value, increases gradually with the applied strain. These results are quite distinct from the piezoresistive effects observed in conventional layered semiconductors,[27,28] which exhibit linearity along both anisotropic axes throughout the entire strain range and are generally attributed to the continuous strain modulation of the bandgap. Notably, the electromechanical responses of the above two devices are reversible and repeatable. The observed disparate dependence indicates the prominent anisotropic resistance response to uniaxial tensile strain, which is considered as the strain-induced reversible MIT behavior of the VO_2(B) single crystal, as discussed in detail below.

In order to shine a light on the anisotropic electromechanical response and confirm the phase transition under uniaxial tensile strain, we studied the optical contrast variation and the simultaneous resistance response in the strained VO_2(B) device. Figure 3(a) presents the evolution of domain patterns imaged at different labeled strains in the device with the channel oriented along the *b*-axis. For visualization, optical images were obtained using the look-up tables (LUTs) mode of the high-magnification optical microscope, thereby giving rise to different levels and highlighting brightness contrast. Below 0.33% strain, the normalized resistance steadily increases without any discernible optical changes [Fig. S3(a)]. When the normalized resistance ramps up under 0.41% strain, the sample shows an abrupt change in optical reflection, with bright (pink) domains nucleating in the original dark (blue) phase. The highly stripe-ordered domains are meandering and generally perpendicular to the channel direction (*b*-axis). It is well known that the MIT in vanadium dioxide is generally accompanied by enormous and sharp changes in the resistivity and optical properties, as previously reported in VO_2(R) beams or films.[9,16,29] The emerging domains in the strained VO_2(B) single crystal confirm the ubiquity of the stripe state, signifying the transition from the metallic phase to the insulating phase. As shown in the optical image under 0.52% strain, while the area of stripy domains expands with increasing strain, triangular domains appear and grow at both long edges of the device, displaying an adjustable coexistence of two phases. Finally, all domains almost merge into a single insulating phase and replace the metallic phase under 0.74% strain, accompanied by a substantial increase in the normalized resistance with respect to the original value.

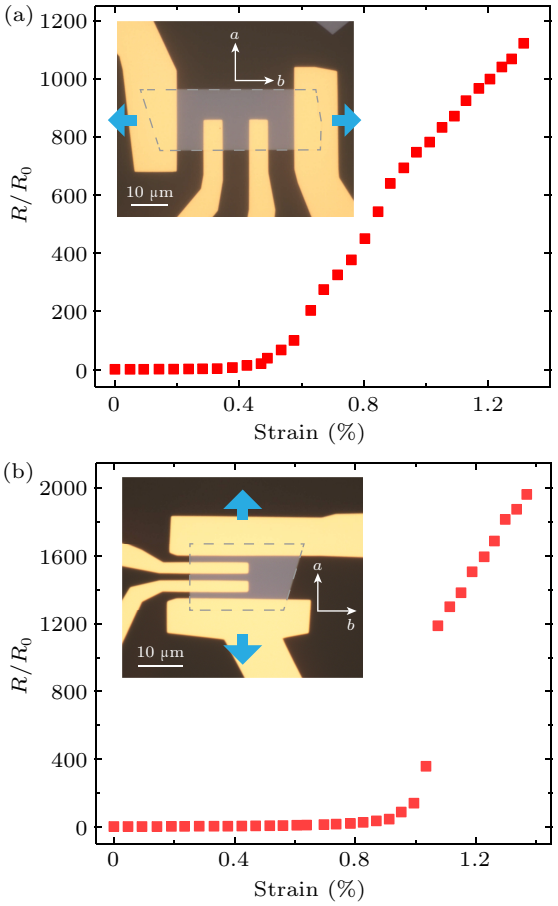


Fig. 2. Normalized resistance as a function of strain for the VO_2(B) devices with the conductive channel oriented along the *b*-axis (a) and the *a*-axis (b), respectively. Insets are optical images of four-terminal devices and the uniaxial tensile strain along the channel direction is labeled as blue arrows.

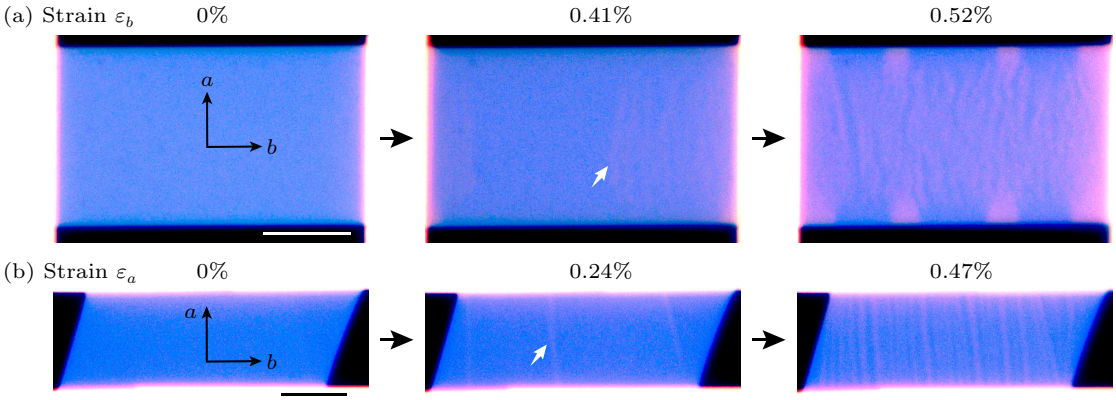


Fig. 3. (a) Series of optical images (in LUTs mode) showing the development of pink insulating domains as the tensile strain along the *b*-axis increases. (b) Optical images (in LUTs mode) of stripe-ordered patterns generating and expanding with increasing strain along the *a*-axis. White arrows highlight the nucleation of stripy domains. Scale bars in panels (a) and (b) are 10 μm.

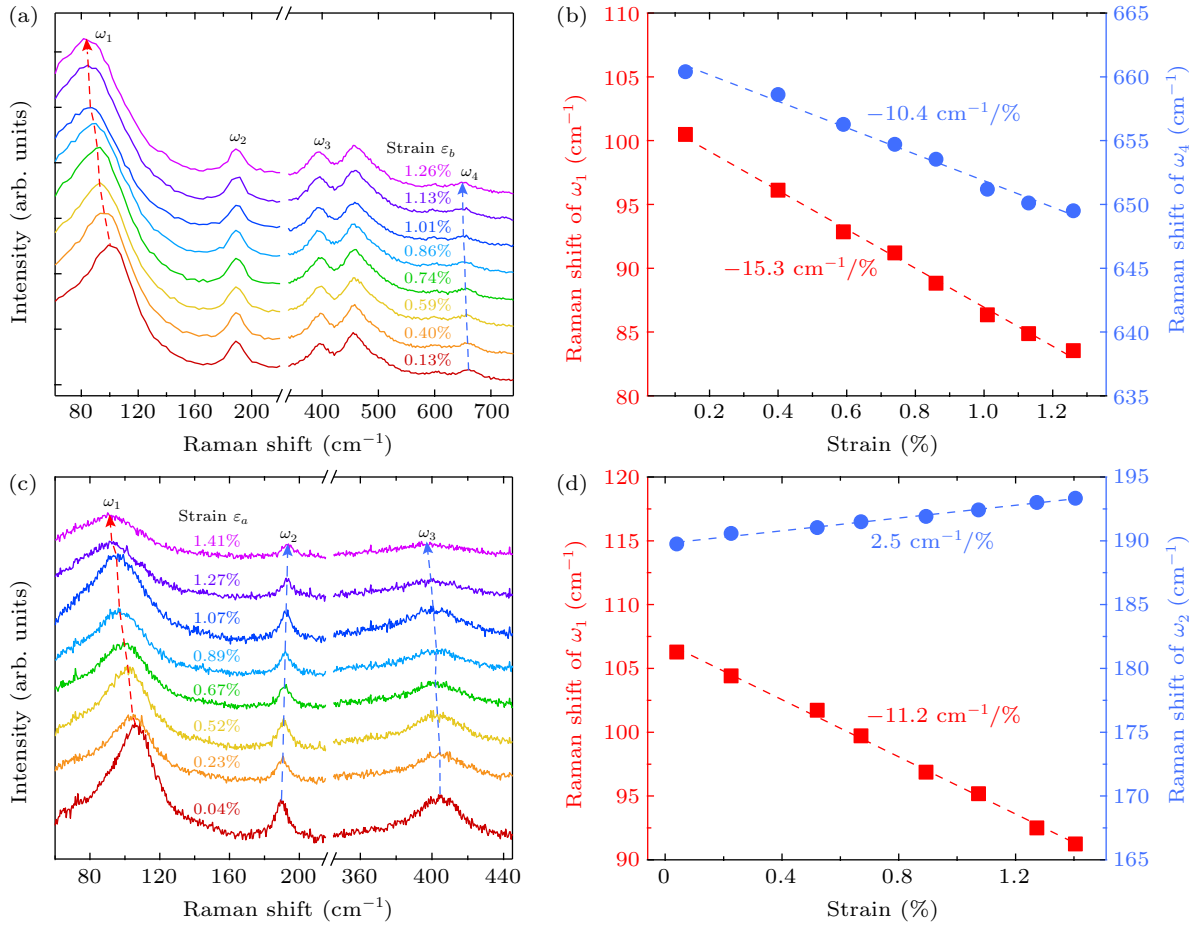


Fig. 4. (a) Raman spectra of a VO_2(B) device under incremental strain along its *b*-axis. (b) Peak positions of the rigid-chain modes (ω_1, left) and the V–O_3 vibration mode (ω_4, right) as a function of strain, extracted from the red and blue dashed arrows in panel (a), respectively. (c) Raman spectra of a VO_2(B) device under increasing strain along its *a*-axis. (d) Corresponding peak positions of the rigid-chain modes (ω_1, left) and the V–O–V bending mode (ω_2, right) in panel (c) as a function of strain, respectively.

As expected, the evolution of the insulating phase is completely different in the device along the *a*-axis. When three straight stripy domains nucleate at a tensile strain of 0.24% [Fig. 3(b)], there is no significant change in the normalized resistance [Fig. S3(b)]. Even though parallel stripes increase substantially as the strain increases to 0.47%, the normalized resistance remains relatively low. Upon reaching 0.65% strain, a dramatic surge in normalized resistance occurs within a narrow strain range of 0.04%, with insulating domains occupying almost the entire conductive channel. Notably, the straight stripes align parallel to the channel direction (*a*-axis). Combined with the results from both types of VO_2(B) devices, we reveal the fact that the applied strain preferentially induces a unidirectional stripe state along the *a*-axis, closely associated with the strain-modulated resistance variation. Moreover, when the tensile strain is released, both samples revert to the initial metallic phase and all stripy domains disappear. By stretching the same VO_2(B) flake along two orthogonal crystal orientations, we acquire the diagonal stripes slightly tilting with respect to the *a*-axis ($\varepsilon_b = 0.42\%$) and the straight stripes running along the *a*-axis ($\varepsilon_a = 0.47\%$), which further verify the strain-induced anisotropic insulating state (Fig. S4).

To gain further insight into the physical origin of the unidirectional insulating stripy domains present in the strained VO_2(B) flake, we investigated the influence of uniaxial tension on Raman spectroscopy. As shown in Fig. 4, the Raman spectra of the VO_2(B) flakes are partially characterized by peaks near 104 cm^{-1}, 189 cm^{-1}, 400 cm^{-1}, 460 cm^{-1}, and 663 cm^{-1}. The observed lowest-frequency peak near 104 cm^{-1} is attributed to the rigid-chain modes, while the other characteristic peaks are related to different V–O bond modes. All these peaks are highly consistent with the Raman signature of monoclinic VO_2(B) reported in previous works.[30–32] With increasing strain along the *b*-axis, both the rigid-chain modes (ω_1) and the V–O_3 vibration mode (ω_4) redshift linearly, as demonstrated in Figs. 4(a) and 4(b). Similarly, a Raman device shows a noticeable redshift of ω_1 under incremental strain along the *a*-axis, as shown in Figs. 4(c) and 4(d). It is noteworthy that the strain-modulated redshift of the rigid-chain modes results from the weakened bonding between rigid-molecule units, i.e., duplex zigzag chains of vanadium atoms.[33,34] Previous studies have shown that the low-frequency vibration modes for vanadium dioxide are bound up with the motion of V–V dimers in vanadium chains.[35,36]

Therefore, we infer that the strain-induced weakened interaction is ascribed to the in-plane V(1)–V(2) dimerization, arising from the deformation of the zigzag chains under the combined influence of uniaxial strain and the Poisson effect. This result contrasts sharply with its low-temperature phase transition, in which the out-of-plane V(2)–V(2) pairing enhances the interaction between adjacent zigzag chains.[17,18] Note that different types of dimerization can serve as a distinguishing characteristic between various insulating phases, as prominently observed in the other two insulating phases (M1 and M2) of vanadium dioxide.[37]

When uniaxial tensile strain is separately applied along two orthogonal crystal axes of VO_2(B), vanadium atoms further deviate from the centers of VO_6 octahedra, which enhances the hybridization of V 3d orbitals with O 2p orbitals (p–d hybridization).[7,8] Moreover, similar in-plane dimerization induces a band gap near the Fermi level, resulting in the emergence of an insulating phase characterized by a significant resistance change and a unidirectional stripe state. As anticipated, we observe diagonal stripes and triangular patterns ($\varepsilon_b = 1.01\%$), or periodic straight stripes ($\varepsilon_a = 1.12\%$), in the aforementioned Raman devices (Fig. S5). The morphological differences in domains may be attributed to the opposite modulation (increasing/decreasing) of the folding angles of zigzag chains under two in-plane uniaxial strains (*b*-axis/*a*-axis), which affects the tilt angles of the V–V dimers. Additionally, in the device along the *a*-axis, there is no obvious variation in ω_4, whereas the V–O–V bending mode (ω_2) exhibits a slight blueshift and the V–O–V stretching mode (ω_3) gradually shifts to a lower frequency as the tensile strain increases. The strain-modulated differences in Raman shifts of these V–O bond modes are derived from the disparate distortions of VO_6 octahedra.

The anisotropic electromechanical response observed during the MIT could arise from the different spatial distributions of insulating domains within the conductive channel. When the VO_2(B) device is stretched along its *b*-axis, the nucleated stripy domains, arranged perpendicularly to the channel direction, can be conceptualized as several large resistors, which restrict electron motion and cause the channel resistance to ramp up distinctly. Based on these features, we propose a series-connection mechanism between the original metallic areas and the insulating stripy domains. In the coexistence of metallic and insulating phases, the proportion of domains gradually scales up with tensile strain, leading to a rapid linear increase in series-connection resistance. Consequently, the synchronous transitions observed in the electrical transport and optical reflection are achieved, and the strain-induced MIT plays a dominant role in the electromechanical response. On the other hand, parallel straight stripes approximately divide the conductive channel into many separate narrow channels in the stretched VO_2(B) device along its *a*-axis. The persistence of integral metallic channels with much smaller resistivity renders the resistance variation insensitive to the nucleation of the insulating stripe state, precisely conforming to a parallel connection of metallic and insulating resistances. Thus, despite a marked increase in the quantity of stripes with the applied strain, the parallel-connection resistance exhibits only a slight increment. Until the entire VO_2(B) flake is almost transformed into the insulating phase under greater strain, a significant surge in channel resistance would arise within an extremely narrow strain range because all narrow metallic channels are severed by emerging insulating domains.

In summary, we report an anisotropic metal–insulator transition in strained single-crystal VO_2(B) devices. By applying uniaxial tensile strain along two orthogonal crystal orientations, respectively, we demonstrate that the electromechanical response is gradual for the *b*-axis while transient for the *a*-axis. Such an anisotropic feature is ascribed to the strain-induced phase transition and the preferential arrangement of the unidirectional stripe state observed in optical reflection. We also carry out the strain-modulated Raman spectrum measurement and reveal that these insulating stripy domains originate from the in-plane V(1)–V(2) dimerization within the distorted zigzag chains of vanadium atoms. The anisotropic electromechanical response of VO_2(B) material uncovered in our work can be utilized for designing orientation-dependent strain sensors and detecting mechanical signals applied along various directions, holding great promise in wearable and robotic applications.

Acknowledgments

Project supported by the National Key R&D Program of China (Grant No. 2023YFF1203600), the National Natural Science Foundation of China (Grant Nos. 62122036, 62034004, 12322407, 61921005, and 12074176), and the Strategic Priority Research Program of the Chinese Academy of Sciences (Grant No. XDB44000000). F.M. would like to acknowledge support from the AIQ Foundation. The microfabrication center of the National Laboratory of Solid State Microstructures (NLSSM) is acknowledged for their technique support. This work was supported by the program for Outstanding PhD Candidates of Nanjing University.

References

[1] Cao J, Ertekin E, Srinivasan V, Fan W, Huang S, Zheng H, Yim J W, Khanal D R, Ogletree D F, Grossman J C and Wu J 2009 *Nat. Nanotechnol.* **4** 732

[2] Tselev A, Luk'yanchuk I A, Ivanov I N, Budai J D, Tischler J Z, Strelcov E, Kolmakov A and Kalinin S V 2010 *Nano Lett.* **10** 4409

[3] Hong B, Yang Y, Hu K, Dong Y, Zhou J, Zhang Y, Zhao W, Luo Z and Gao C 2019 *Appl. Phys. Lett.* **115** 251605

[4] Liu K, Lee S, Yang S, Delaire O and Wu J 2018 *Mater. Today* **21** 875

[5] Shvets P, Dikaya O, Maksimova K and Goikhman A 2019 *J. Raman Spectrosc.* **50** 1226

[6] Hu P, Hu P, Vu T D, Li M, Wang S, Ke Y, Zeng X, Mai L and Long Y 2023 *Chem. Rev.* **123** 4353

[7] Aetukuri N B, Gray A X, Drouard M, Cossale M, Gao L, Reid A H, Kukreja R, Ohldag H, Jenkins C A, Arenholz E, Roche K P, Dürr H A, Samant M G and Parkin S S P 2013 *Nat. Phys.* **9** 661

[8] Fan L L, Chen S, Luo Z L, Liu Q H, Wu Y F, Song L, Ji D X, Wang P, Chu W S, Gao C, Zou C W and Wu Z Y 2014 *Nano Lett.* **14** 4036

[9] Liu M K, Wagner M, Abreu E, Kittiwatanakul S, McLeod A, Fei Z, Goldflam M, Dai S, Fogler M M, Lu J, Wolf S A, Averitt R D and Basov D N 2013 *Phys. Rev. Lett.* **111** 096602

[10] Yang M, Yang Y, Bin H, Wang L, Hu K, Dong Y, Xu H, Huang H, Zhao J, Chen H, Song L, Ju H, Zhu J, Bao J, Li X, Gu Y, Yang T, Gao X, Luo Z and Gao C 2016 *Sci. Rep.* **6** 23119

[11] Hu K, Yang Y, Hong B, Zhao J, Luo Z, Li X, Zhang X, Gu Y, Gao X and Gao C 2017 *J. Alloys Compd.* **699** 575

[12] Jones A C, Berweger S, Wei J, Cobden D and Raschke M B 2010 *Nano Lett.* **10** 1574

[13] Hu B, Ding Y, Chen W, Kulkarni D, Shen Y, Tsukruk V V and Wang Z L 2010 *Adv. Mater.* **22** 5134

[14] Cao J, Gu Y, Fan W, Chen L Q, Ogletree D F, Chen K, Tamura N, Kunz M, Barrett C, Seidel J and Wu J 2010 *Nano Lett.* **10** 2667

[15] Guo H, Chen K, Oh Y, Wang K, Dejoie C, Syed Asif S A, Warren O L, Shan Z W, Wu J and Minor A M 2011 *Nano Lett.* **11** 3207

[16] Park J H, Coy J M, Kasirga T S, Huang C, Fei Z, Hunter S and Cobden D H 2013 *Nature* **500** 431

[17] Oka Y, Yao T, Yamamoto N, Ueda Y and Hayashi A 1993 *J. Solid State Chem.* **105** 271

[18] Corr S A, Grossman M, Shi Y, Heier K R, Stucky G D and Seshadri R 2009 *J. Mater. Chem.* **19** 4362

[19] Lourembam J, Srivastava A, La-o-vorakiat C, Rotella H, Venkatesan T and Chia E E 2015 *Sci. Rep.* **5** 9182

[20] Popuri S R, Artemenko A, Decourt R, Josse M, Chung U C, Michau D, Maglione M, Villesuzanne A and Pollet M 2015 *J. Phys. Chem. C* **119** 25085

[21] Lourembam J, Srivastava A, La-o-Vorakiat C, Cheng L, Venkatesan T and Chia E E M 2016 *Sci. Rep.* **6** 25538

[22] Zhang Y, Wang X, Zhou Y, Lai H, Liu P, Chen H, Wang X and Xie W 2021 *Nano Lett.* **22** 485

[23] Wang Y, Zhu J, Yang W, Wen T, Pravica M, Liu Z, Hou M, Fei Y, Kang L, Lin Z, Jin C and Zhao Y 2016 *Nat. Commun.* **7** 12214

[24] Théobald F, Cabala R and Bernard J 1976 *J. Solid State Chem.* **17** 431

[25] Liu J, Li Q, Wang T, Yu D and Li Y 2004 *Angew. Chem. Int. Ed.* **43** 5048

[26] Wang Y, Wang C, Liang S J, Ma Z C, Xu K, Liu X W, Zhang L L, Admasu A S, Cheong S W, Wang L Z, Chen M Y, Liu Z L, Cheng B, Ji W and Miao F 2020 *Adv. Mater.* **32** 2004533

[27] Zhang Z, Li L, Horng J, Wang N Z, Yang F, Yu Y, Zhang Y, Chen G, Watanabe K, Taniguchi T, Chen X H, Wang F and Zhang Y 2017 *Nano Lett.* **17** 6097

[28] An C, Xu Z, Shen W, Zhang R, Sun Z, Tang S, Xiao Y F, Zhang D, Sun D, Hu X, Hu C, Yang L and Liu J 2019 *ACS Nano* **13** 3310

[29] Shi R, Chen Y, Cai X, Lian Q, Zhang Z, Shen N, Amini A, Wang N and Cheng C 2021 *Nat. Commun.* **12** 4214

[30] Wang X J, Li H D, Fei Y J, Wang X, Xiong Y Y, Nie Y X and Feng K A 2001 *Appl. Surface Sci.* **177** 8

[31] Huang C, Chen L, Xu G and Miao L 2012 *J. Sol-Gel Sci. Technol.* **63** 103

[32] Zhang S, Fu J, Su Q, Wu L and Li X 2016 *Rare Metal Mater. Eng.* **45** 1374

[33] Zallen R and Slade M 1974 *Phys. Rev. B* **9** 1627

[34] Hsueh H C, Warren M C, Vass H, Ackland G J, Clark S J and Crain J 1996 *Phys. Rev. B* **53** 14806

[35] Chen Y, Zhang S, Ke F, Ko C, Lee S, Liu K, Chen B, Ager J W, Jeanloz R, Eyert V and Wu J 2017 *Nano Lett.* **17** 2512

[36] Lee D, Chung B, Shi Y, Kim G Y, Campbell N, Xue F, Song K, Choi S Y, Podkaminer J P, Kim T H, Ryan P J, Kim J W, Paudel T R, Kang J H, Spinuzzi J W, Tenne D A, Tsymbal E Y, Rzchowski M S, Chen L Q, Lee J and Eom C B 2018 *Science* **362** 1037

[37] Sohn J I, Joo H J, Ahn D, Lee H H, Porter A E, Kim K, Kang D J and Welland M E 2009 *Nano Lett.* **9** 3392